Publishing Excellence
Inspiring Progress
ARISTON PUBLICATIONS
ChemSci Advances
ISSN: 2997-9587 www.aristonpubs.com/chemsci-advances https://doi.org/10.69626/csa.2024.0139

RESEARCH ARTICLE

Structural and Morphological Investigation of CoZnFe – Oxide Nanoparticles and Their Electrical and Magnetic Properties

Ram S. Barkule [1,*], Sudarshana G. Badhe[2], Mahendra D. Shelar[3]

ABSTRACT: Spinel ferrites ($MeFe_2O_4$) with divalent cations like Co^{2+} and Zn^{2+} exhibit unique crystal structures and magnetic properties, making them essential in various applications. This study focuses on CoZnFe-oxide nanoparticles (NPs), synthesized using a wet chemical method. X-ray diffraction (XRD) confirmed a single-phase cubic spinel structure, while scanning electron microscopy (SEM) revealed clustered, spherical nanoparticles with rough surfaces. Fourier-transform infrared (FTIR) spectroscopy identified absorption peaks corresponding to metal-oxygen bond vibrations. DC resistivity measurements indicated thermally activated conduction behavior, typical of semiconductors. Magnetic analysis through an M-H plot confirmed ferromagnetic behavior with significant saturation magnetization, coercivity, and remanence. These findings demonstrate the structural, electrical, and magnetic characteristics of $Co_{0.8}Zn_{0.2}Fe_2O_4$ nanoparticles, highlighting their potential in semiconductor technology, nanosensors, biomedical applications, and more.

Keywords: Spinel ferrites, CoZnFe, Structural properties, Magnetic properties.

Received: 03 April 2024; Revised: 17 May 2024; Accepted: 07 June 2024; Published Online: 27 June 2024

1. INTRODUCTION

Spinel ferrites, represented by the general formula $MeFe_2O_4$, where Me can be divalent cations such as Fe^{2+}, Co^{2+}, Ni^{2+}, Cu^{2+}, Mg^{2+}, or Zn^{2+}, are characterized by their unique crystal structures and magnetic properties. The formula for spinel ferrites can be expanded to $(Me^{2+}_{1-x}Fe^{3+}_{x})[Me^{2+}_{x}Fe^{3+}_{2-x}]O_4$, with cation distribution within the crystal lattice defining the type of cubic structure: normal, inverse, or mixed spinel. In a normal spinel, divalent cations occupy tetrahedral (A) sites while trivalent cations fill the octahedral [B] sites [1]. Conversely, in an inverse spinel, trivalent cations are in the (A) sites and a mixture of divalent and trivalent cations occupy the [B] sites. Mixed spinels show no strong preference for cation occupation at either site [2]. For instance, cobalt ferrite ($CoFe_2O_4$) exhibits an inverse spinel structure with trivalent iron ions (Fe^{3+}) in the tetrahedral sites and both divalent cobalt ions (Co^{2+}) and trivalent iron ions (Fe^{3+}) in the octahedral sites, with oxygen anions forming a face-centered cubic lattice.

Cobalt zinc ferrite nanoparticles have attracted significant research interest due to their applications in semiconductor technology, nanosensors, catalytic activities, choke coils, nanorobotic devices, biomedical applications such as MRI contrast agents, and as pigments [3]. These versatile applications underscore the importance of cobalt zinc ferrite nanoparticles in advancing technology and improving various industrial and medical processes.

Ongoing research continues to explore and expand the potential uses of spinel ferrites, making them a crucial area of study in materials science and nanotechnology [4], drug delivery [5], microwave-absorbing materials [6], and electronic devices [7]. Ferrites, known for their magnetic properties and versatility, are extensively used in a variety of

[1] Department of Physics, Sundarrao More Arts, Commerce and Science College, Poladpur, Raigad, 402303 India
[2] Department of Physics, R.B. Attal Arts, Science and Commerce College, Georai, Beed, 431127 India
[3] Department of Chemistry, Rajarshi Shahu Art's, Commerce and Science College, Pathri, 431111 India

*Authors to whom correspondence should be addressed:
rambarkule@gmail.com (R. S. Barkule)

applications including transformers, inductors, noise filters, high-density recording media, recording heads, and magnetic carriers [8].

Nanostructured spinel ferrites can be synthesized using various wet chemical methods, including the ceramic method [9], co-precipitation [10], sol-gel auto-combustion [11], and hydrothermal processing, each offering unique advantages based on application needs [12]. Among these, the sol-gel auto-combustion method is particularly effective for producing spinel ferrite nanoparticles due to its simplicity, chemical homogeneity, low synthesis temperature, cost-effectiveness, rapid processing, and environmental friendliness. It allows precise stoichiometric control and narrow particle size distribution, producing nanoparticles with sizes typically ranging from 10 to 50 nm. For example, the synthesis of cobalt zinc ferrite ($Co_xZn_{1-x}Fe_2O_4$) nanoparticles via this method involves temperatures of 300-500°C, significantly lower than traditional methods, and yields high saturation magnetization and coercivity values. This advanced control over material properties has enabled the development of high-performance devices and materials. Applications of cobalt zinc ferrite nanoparticles are broad, including uses in semiconductor technology, nanosensors, catalysis, electronic circuits, and biomedical fields such as drug delivery and MRI contrast enhancement. Their versatility and effectiveness underscore the importance of ongoing research in advancing the field of spinel ferrites [13, 14]

Fe^{3+}: ↑ ↑ ↑ ↑ ↑
d-orbitals (5 electrons)
Fe^{2+}: ↑ ↓ ↑ ↑ ↑ ↑
d-orbitals (6 electrons)
Co^{2+}: ↑ ↓ ↑ ↓ ↑ ↑ ↑
d-orbitals (7 electrons)
Zn^{2+}: ↑ ↓ ↑ ↓ ↑ ↓ ↑ ↓ ↑ ↓
d-orbitals (10 electrons)

The electron configurations of different metal ions commonly found in spinel ferrites significantly influence their magnetic and electronic properties. For Fe^{3+} (Ferric ion), the configuration is depicted as five unpaired 3d electrons (↑ ↑ ↑ ↑ ↑), reflecting its $[Ar]3d^5$ configuration after losing three electrons. This high-spin state contributes to its strong magnetic properties. Fe^{2+} (Ferrous ion) shows a configuration with four unpaired electrons and one paired (↑↓ ↑ ↑ ↑ ↑), corresponding to its $[Ar]3d^6$ state after losing two electrons, which also affects its magnetic characteristics. Co^{2+} (Cobaltous ion) has a configuration with three unpaired electrons and two paired (↑↓ ↑↓ ↑ ↑ ↑), resulting from its $[Ar]3d^7$ state after losing two electrons. This arrangement plays a crucial role in the magnetic behavior of cobalt ferrite. Zn^{2+} (Zinc ion), on the other hand, has a fully paired electron configuration (↑↓ ↑↓ ↑↓ ↑↓ ↑↓) in its $[Ar]3d^{10}$ state after losing two electrons, leading to diamagnetic properties due to the absence of unpaired electrons. These varied electron configurations in metal ions like Fe^{3+}, Fe^{2+}, Co^{2+}, and Zn^{2+} in spinel ferrites determine the material's overall magnetic and electronic properties, making them suitable for diverse applications in electronic devices, magnetic storage, and biomedical fields [15, 16].

This study focuses on CoZnFe-oxide NPs, synthesized using a wet chemical method and characterized by various techniques. Finally, the electrical and magnetic properties of the synthesized nanoparticles were examined.

2. EXPERIMENTAL DETAILS

2.1. Materials and methods

For the synthesis of spinel-structured $Co_{1-x}Zn_xFe_2O_4$ nanoparticles with varying compositions where x ranges from 0.2 to 0.8), starting materials including cobalt nitrate hexahydrate ($Co(NO_3)_2·6H_2O$), zinc nitrate tetrahydrate ($Zn(NO_3)_2·4H_2O$), and ferric nitrate nonahydrate ($Fe(NO_3)_3·9H_2O$), each with a purity of 99.9%, were utilized without further purification. The synthesis process involved the use of citric acid as a complexing agent to facilitate the formation of the desired spinel structure. The ratio of metal nitrates to the fuel (citric acid) was carefully maintained at 1:3 to ensure optimal reaction conditions. Additionally, ammonia solution (NH_4OH) was employed to adjust and stabilize the pH at 8 throughout the synthesis, which is crucial for achieving the desired properties and composition of the nanoparticles. This controlled approach allows for precise tuning of the nanoparticles' composition and properties, contributing to the successful production of $Co_{1-x}Zn_xFe_2O_4$ nanoparticles with tailored characteristics for various applications.

2.2. Synthesis of $CoZnFe_2O_4$ nanoparticles

The wet chemical synthesis was designed to synthesize $CoZnFe_2O_4$ nanoparticles (NPs). Metal nitrates of cobalt and ferric, both with 99.9% purity, were mixed together in a beaker with an adequate amount of deionized (DI) water. The resulting solution was rigorously stirred and homogenized on a magnetic hot-plate stirrer. A 1:3 ratio of metal nitrates to citric acid ($C_6H_5O_7^{3-}$) was used as the complexing agent. Water evaporation was achieved by setting the hot-plate temperature to 80°C for 3 hours. Ammonia solution (NH_4OH) was added slowly to maintain the solution's pH at 8. During the intermediate stage, the solution transitioned from a ‘sol’ to a ‘gel,’ eventually forming a ‘viscous brown gel.’ In the final stage, increased ionic exchange within the system led to the release of gaseous by products. The temperature was raised to 110°C to initiate self-propagating auto-combustion, resulting in a loose powder of pre-sintered $CoZnFe_2O_4$.

3. RESULTS AND DISCUSSION

3.1. XRD of CoZnFe-oxide NPs

Structural studies of $CoZnFe_2O_4$ nanoparticles (NPs) were performed using X-ray diffraction (XRD) with a X'PertPRO MPD PANAlytical system. The analysis was conducted over a 2θ range of 20º to 80º using Cu-Kα radiation with a wavelength of λ = 1.5405 Å at room temperature.

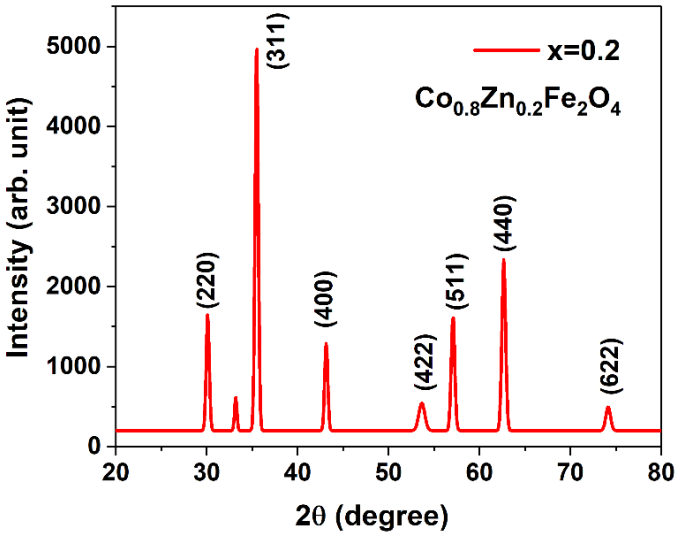

Fig. 1. X-ray diffraction pattern of CoZnFe-oxide NPs for x=0.2.

The XRD pattern is shown in Figure 1 that indicated that the $CoZnFe_2O_4$ NPs exhibited a single-phase cubic spinel structure, with no secondary peaks observed. The diffraction pattern confirmed the presence of specific planes, including (220), (311), (400), (422), (511), (440), and (622), as detailed in Table 1. The X-ray diffraction (XRD) data table provides a detailed analysis of the crystal structure of the material, revealing the presence of a spinel-type structure [17]. The table lists the Miller indices (h, k, l) for various diffraction peaks, along with their corresponding 2θ values, interplanar spacings (d), and lattice parameters (a). The Miller indices indicate the orientation of the crystal planes responsible for the observed diffraction peaks. For instance, the peak at 2θ = 30.109° corresponds to the (220) plane, while the peak at 2θ = 35.492° is attributed to the (311) plane [18]. The calculated d-spacing, which range from 1.277 Å for the (622) plane to 2.965 Å for the (220) plane, are consistent with the expected values for a spinel ferrite material.

The lattice parameter (a) remains relatively constant, with an average value of 8.390 Å, suggesting a well-defined cubic spinel structure. The ratio of the lattice parameter to the d-spacing squared, $(a/d)^2$, provides further evidence of the spinel structure, as the values are consistent with those reported for similar ferrite materials. Overall, the XRD data confirms the successful synthesis of a single-phase spinel ferrite with a well-defined cubic structure [19].

The X-ray diffraction (XRD) data presented in Table 2 provides a comprehensive analysis of the crystallographic properties of the material, revealing valuable insights into its structure and quality. The 2θ values, ranging from 30.10° to 74.15°, correspond to specific crystal planes within the material's lattice, with the most prominent peaks occurring at 35.49°, 43.14°, and 57.08°. The FWHM (Full Width at Half Maximum) values, which are consistently below 1° in both degrees and radians, indicate sharp, well-defined peaks, suggesting a high degree of crystallinity in the material. The calculated Cos θ values, which decrease with increasing 2θ, are used in the Scherrer equation to determine the average crystallite size (D) for each peak. The crystallite sizes vary from 11.57 nm for the peak at 53.65° to 21.55 nm for the peak at 43.14°, with an overall average of 18.584 nm.

Table 3 provides a dislocation density (δ), lattice strain (ε), of the CoZnFe-oxide NPs. The dislocation density (δ) values, which range from $2.152*10^3$ to $7.468*10^3$ nm^{-2}, provide an estimate of the number of defects present in the crystal structure, while the microstrain (ε) values, ranging from $0.465*10^{-3}$ to $1.978*10^{-3}$, quantify the internal strain within the crystallites.

Table 1. Miller indices of the CoZnFe-oxide NPs typical sample x = 0.2.

h	k	l	2θ	θ	Sinθ	2Sinθ	d	(a/d)^2	a
2	2	0	30.109	15.054	0.260	0.520	2.965	7.988	8.386
3	1	1	35.492	17.746	0.305	0.610	2.527	11.000	8.380
4	0	0	43.141	21.571	0.368	0.735	2.095	16.005	8.379
4	2	2	53.655	26.828	0.451	0.903	1.706	24.118	8.360
5	1	1	57.083	28.542	0.478	0.956	1.612	27.032	8.375
4	4	0	62.669	31.335	0.520	1.040	1.481	32.022	8.377
6	2	2	74.155	37.077	0.603	1.206	1.277	43.039	8.473
									8.390

Table 2. FWHM, Crystallite size (D), dislocation density (δ), lattice strain (ε), of the CoZnFe-oxide NPs.

2θ	FWHM Radian (θ)	Cos θ	D= 0.9λ/ βCosθ	D nm
30.10	0.007	0.966	207.41	20.74
35.49	0.007	0.952	204.71	20.47
43.14	0.007	0.930	215.54	21.55
53.65	0.013	0.892	115.71	11.57
57.08	0.008	0.879	197.41	19.74
62.66	0.008	0.854	194.00	19.40
74.15	0.010	0.798	166.05	16.60
				18.584

Table 3. Dislocation density (δ), lattice strain (ε), of the CoZnFe-oxide NPs.

2θ	$\delta*10^3$ (nm^{-2})	$\varepsilon*10^{-3}$
30.10	2.324	0.465
35.49	2.386	0.569
43.14	2.152	0.684
53.65	7.468	1.698
57.08	2.565	1.087
62.66	2.656	1.274
74.15	3.626	1.978

These results demonstrate the high quality and well-defined crystallographic structure of the material, making it suitable for various applications that require a high degree of crystallinity and low defect concentrations.

The crystallite size (D) of CoZnFe-oxide NPs was estimated from the FWHM of the peak (311) in all the reflections by using the Debye-Scherrer formula mentioned below [20]:

$$D = 0.89\lambda/\beta cos\theta$$

Where β = FWHM of the diffraction peak corresponding to the plane (311) [21], λ = wavelength of X-ray, θ = 0.89 (diffraction angle), and that is also considered as a Scherrer's constant. The obtained results confirmed the nanosize formation. The XRD pattern of $Co_{0.8}Zn_{0.2}Fe_2O_4$ (x=0.2) unequivocally demonstrates the crystalline nature of the material. The presence of sharp, distinct peaks in the diffraction pattern is indicative of a well-ordered atomic arrangement within the sample. Each peak corresponds to specific crystallographic planes, as defined by their Miller indices, and their positions on the 2θ axis provide crucial information about the lattice parameters of the crystal structure. Moreover, the relative intensities of these peaks offer valuable insights into the orientation and abundance of various crystallographic planes, contributing to a comprehensive understanding of the material's structural properties.

3.2. Microstructure of CoZnFe-oxide NPs

The SEM was carried out by FEG-Scanning electron micrograph Model-JSM-7600F at SAIF IITB Mumbai. The scanning electron microscopy (SEM) image of CoZnFe-oxide nanoparticles (NPs) for x = 0.2 in Figure 2 reveals several important morphological characteristics. The nanoparticles exhibit a clustered and agglomerated morphology, appearing predominantly spherical in shape with rough surfaces. This clustering suggests a tendency for agglomeration, which may be attributed to factors such as surface energy and magnetic interactions between the particles. Additionally, the size distribution of the nanoparticles is relatively broad, indicating the presence of both larger clusters and smaller individual nanoparticles. This variability in size suggests that the synthesis process may not have been perfectly controlled, leading to differences in nanoparticle growth during synthesis. The rough and uneven surface features of the nanoparticles are noteworthy, as they indicate a degree of porosity that could enhance the surface area available for reactions. This increased surface area may be beneficial for various applications, including catalysis and drug delivery, where enhanced interactions with the surrounding environment are desirable. Overall, the SEM observations provide valuable insights into the morphology and potential functionality of the CoZnFe-oxide nanoparticles, highlighting both their structural characteristics and implications for practical

applications.

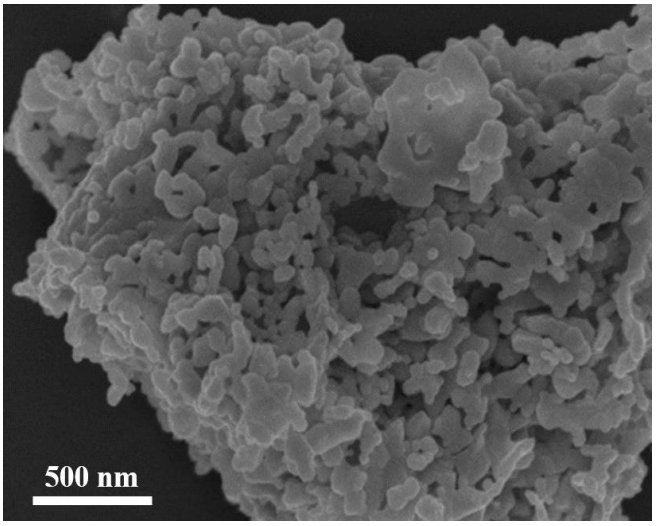

Fig. 2. SEM image of CoZnFe-oxide NPs for x = 0.2.

3.3. Topology of CoZnFe-oxide NPs

The topological investigation of CoZnFe-oxide NPs was carried out by atomic force microscopy (AFM; PARK Model-XE 7); Head mode NC set at point 17.69 nm, amplitude 30.94 nm, frequency 309.68E3 Hz with the scanning rate of 0.5 Hz. AFM images of CoZnFe-oxide NPs have been depicted in Figure 3. According to Hook's law, the atomic force micrography works on the principle of Wonder-Wall forces. These Wonder-Wall forces produced in the atomic structure at the surface of the materials. The intense laser reflections were used to determine the roughness, smoothness, texture property, etc. was seen not to be uniform. [22, 23].

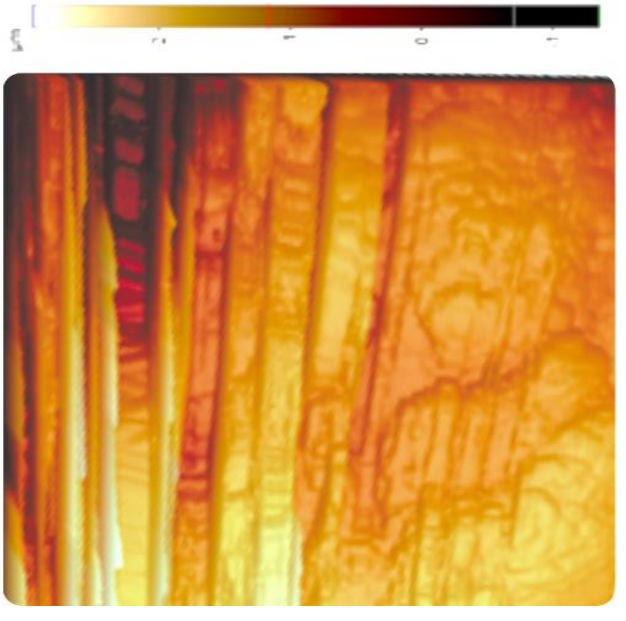

Fig. 3. AFM of CoZnFe-oxide NPs.

3.4. FTIR of CoZnFe-oxide NPs

The FTIR spectra for CoZnFe-oxide nanoparticles with a composition of x = 0.2, as illustrated in the Figure 4, exhibit several significant absorption peaks that elucidate the structural and chemical properties of the material. The initial absorption band (ν_1) detected at approximately 543 cm^{-1} is associated with the stretching vibrations of the metal-oxygen (M-O) bond located at the tetrahedral site. The subsequent absorption band (ν_2), observed at a lower wavenumber of around 402 cm^{-1}, is linked to the octahedral M-O stretching vibration [24]. The intensity and positioning of these absorption bands indicate the impact of Zn substitution on the structural characteristics of the ferrite. The FTIR spectra confirm the presence of spinel ferrite structures, with variations indicating the effective incorporation of Zn into the lattice. These results offer significant insights into the synthesis and potential applications of these ferrite nanoparticles [25].

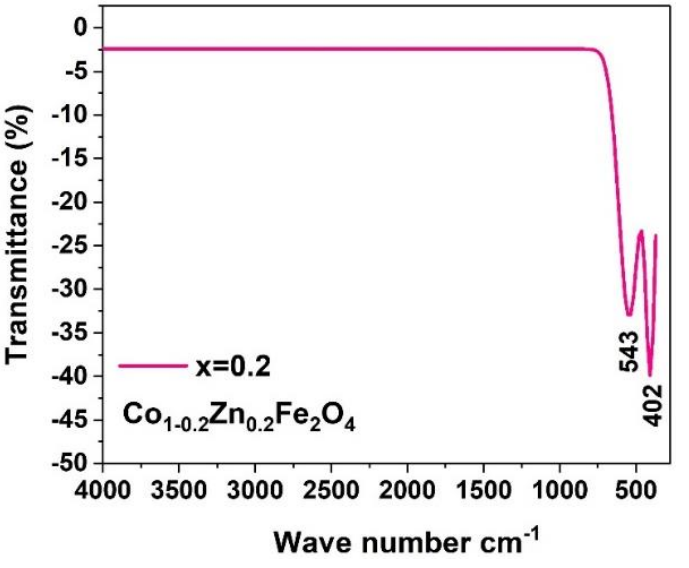

Fig. 4. FTIR spectra of CoZnFe-oxide NPs for x = 0.2.

3.5. DC-resistivity of CoZnFe-oxide NPs

The DC resistivity graph for CoZnFe-oxide nanoparticles with a composition of x = 0.2 provides significant insights into the electrical characteristics of the material. The graph Figure 5 illustrates the natural logarithm of electrical conductivity (log σ) plotted against the reciprocal of temperature (1000/T in Kelvin), revealing a distinct temperature dependence. As the temperature rises (moving from right to left along the x-axis), the electrical conductivity increases, which signifies a reduction in resistivity. This linear correlation indicates an Arrhenius-type behavior, where conductivity rises exponentially with temperature. The slope of the line can be utilized to calculate the activation energy (E_a) for conduction, in accordance with the Arrhenius equation [26]:

$$\sigma = \sigma_0 \exp(\frac{E_a}{kT})$$

This behavior suggests a thermally activated conduction mechanism, characteristic of semiconductors, where charge carriers acquire adequate thermal energy to surpass the activation energy barrier for conduction. The specific composition of $Co_{0.8}Zn_{0.2}Fe_2O_4$ implies that the substitution of Zn has a considerable impact on the conduction mechanism [27]. Zn ions, possessing a different electronic configuration than Co ions, influence the electronic structure and the activation energy for conduction. This substitution modifies the density of states, the mobility of charge carriers, and the overall crystal structure, thereby affecting the conductivity. The DC resistivity graph substantiates that $Co_{0.8}Zn_{0.2}Fe_2O_4$ demonstrates thermally activated semiconducting behavior, with conductivity increasing with temperature, and emphasizes the influence of Zn substitution on the electrical properties of the material [28].

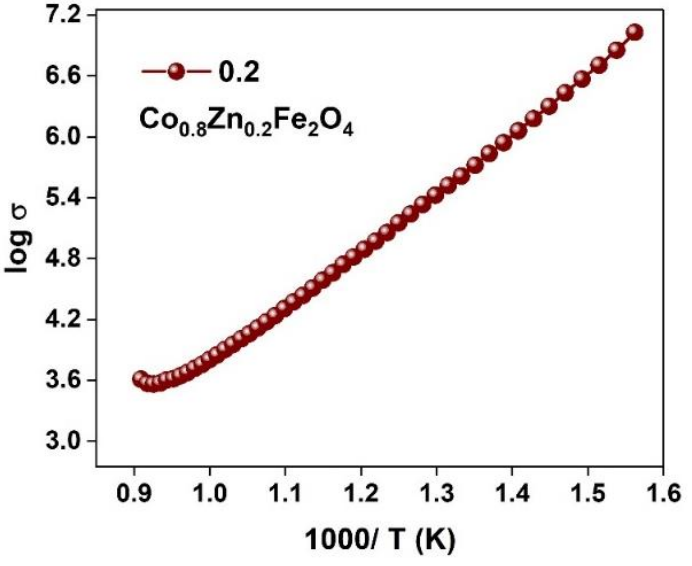

Fig. 5. DC-resistivity of CoZnFe-oxide NPs for x = 0.2.

3.6. Magnetic Property of CoZnFe-oxide NPs

The M-H plot for CoZnFe-oxide nanoparticles with a composition of x = 0.2 provides valuable insights into the material's magnetic properties. The plot exhibits a typical S-shaped hysteresis loop, characteristic of ferromagnetic materials, indicating strong magnetic interactions.

In Figure 6, the saturation magnetization (Ms) is approximately 0.6 emu, representing the maximum magnetization achieved when all magnetic moments align with the applied field. The coercivity (Hc), the field strength required to reduce the magnetization to zero after saturation, is evident from the points where the curve crosses the x-axis. The remanent magnetization (Mr), the residual magnetization when the applied field is reduced to zero, is around 0.3 emu. The significant coercivity and remanence confirm the ferromagnetic behavior of $Co_{0.8}Zn_{0.2}Fe_2O_4$ at room temperature. The hysteresis loop shape and size suggest strong magnetic interactions typical of spinel ferrites. Zn substitution influences the magnetic properties by affecting the cation distribution between the tetrahedral and octahedral sites in the spinel structure. This substitution impacts the overall magnetic behavior, confirming that $Co_{0.8}Zn_{0.2}Fe_2O_4$ is a ferromagnetic material with distinctive magnetic properties due to Zn incorporation [29, 30].

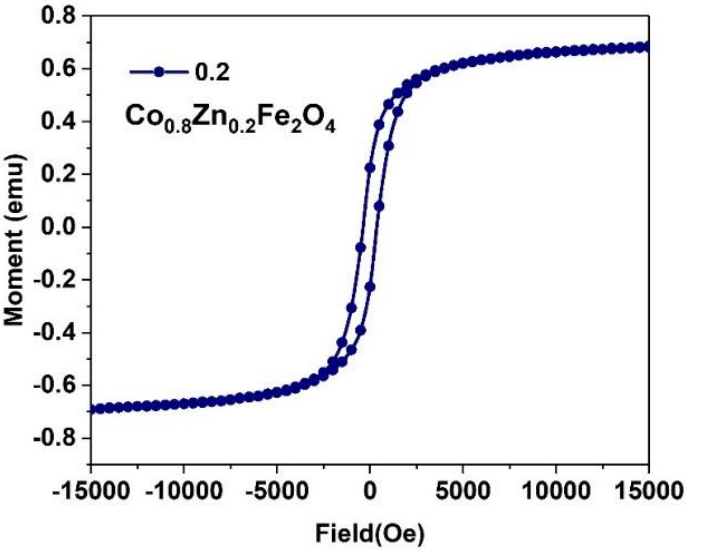

Fig. 6. Magnetic Hysteresis loop of CoZnFe-oxide NPs for x = 0.2.

4. CONCLUSION

Spinel ferrites, represented by the general formula $MeFe_2O_4$, where Me can be divalent cations such as Fe^{2+}, Co^{2+}, Ni^{2+}, Cu^{2+}, Mg^{2+}, or Zn^{2+}, exhibit unique crystal structures and magnetic properties. The structural variations, including normal, inverse, or mixed spinel types, are dictated by the cation distribution within the lattice. For instance, cobalt ferrite ($CoFe_2O_4$) typically displays an inverse spinel structure, while Zn substitution can lead to significant changes in the material's properties. The synthesis of $CoZnFe_2O_4$ nanoparticles was achieved through a wet chemical method, resulting in a single-phase cubic spinel structure as confirmed by XRD analysis. The nanoparticles exhibited a crystalline nature with well-defined peaks and minimal defects, indicating high quality and suitability for various applications. SEM and AFM analyses revealed a clustered and agglomerated morphology with rough surfaces, suggesting potential for enhanced surface interactions in catalytic and biomedical applications. FTIR spectra confirmed the presence of spinel ferrite structures and indicated successful Zn incorporation, which influenced the material's structural characteristics. The DC resistivity analysis demonstrated a thermally activated conduction mechanism, characteristic of semiconductors, with conductivity increasing exponentially with temperature. The

magnetic properties of $CoZnFe_2O_4$ nanoparticles were elucidated through M-H plot analysis, revealing ferromagnetic behavior with significant saturation magnetization, coercivity, and remanence. The Zn substitution influenced the cation distribution and, consequently, the magnetic interactions within the spinel structure. The comprehensive analysis of $CoZnFe_2O_4$ nanoparticles highlights their potential in various technological and industrial applications, including semiconductor technology, nanosensors, catalytic activities, biomedical applications, and more. The ongoing research into spinel ferrites continues to expand their applicability, underscoring their importance in materials science and nanotechnology.

CONFLICT OF INTEREST

The authors declare that there is no conflict of interests.

REFERENCES

[1] Narang, S.B. and Pubby, K., **2021.** Nickel spinel ferrites: a review. *Journal of Magnetism and Magnetic Materials*, 519, p.167163.

[2] Qin, H., He, Y., Xu, P., Huang, D., Wang, Z., Wang, H., Wang, Z., Zhao, Y., Tian, Q. and Wang, C., **2021.** Spinel ferrites (MFe2O4): Synthesis, improvement and catalytic application in environment and energy field. *Advances in Colloid and Interface Science*, 294, p.102486.

[3] Raut, A.V., Khirade, P.P., Shengule, D. and Jadhav, K., **2021.** 50 kGy–100 kGy 60Co γ-irradiation effects on structural and DC-electrical properties of sol–gel synthesized ZnF NPs. *Journal of Materials Science: Materials in Electronics*, 32, pp.11017-11027.

[4] Sambhudevan, S., **2021.** Ferrite-based polymer nanocomposites as shielding materials: A review. *Chemical Papers*, 75, pp.3697-3710.

[5] Kurian, M. and Thankachan, S., **2021.** Structural diversity and applications of spinel ferrite core-shell nanostructures, A review. *Open Ceramics*, 8, p.100179.

[6] Aherrao, D.S., Singh, C. and Srivastava, A., **2022.** Review of ferrite-based microwave-absorbing materials: Origin, synthesis, morphological effects, dielectric/magnetic properties, composites, absorption mechanisms, and optimization. *Journal of Applied Physics*, 132, p. 240701.

[7] Yadav, R.S., Kuřitka, I. and Vilčáková, J., **2020.** Advanced spinel ferrite nanocomposites for electromagnetic interference shielding applications. *Elsevier*, Oxford, United Kingdon.

[8] Raut, A.V., Barote, V.K., Barkule, R.S., Parlikar, R.R., Shengule, D., **2022.** Thermogravimetric analysis, Rietveld refinement, and atomic force micrography of cobalt ferrite nanoparticles exposed to 100 kGy Co60 γ-rays. *Materials Today: Proceedings*, 67, pp.66-71.

[9] Kurian, M., **2023.** Green synthesis routes for spinel ferrite nanoparticles: a short review on the recent trends. *Journal of the Australian Ceramic Society*, 59, pp.1161-1175.

[10] Sarveena, G., Kumar, N., Kondal, M., Singh, M. and Sharma, S.K., **2021.** Wet Chemical Synthesis and Processing of Nanoferrites in Terms of Their Shape, Size and Physiochemical Properties. In: Sharma, S.K. (eds) Spinel Nanoferrites. Topics in Mining, Metallurgy and Materials Engineering. Springer, Cham. pp.63-84.

[11] Diodati, S., Walton, R.I., Mascotto, S. and Gross, S., **2020.** Low-temperature wet chemistry synthetic approaches towards ferrites. *Inorganic Chemistry Frontiers*, 7, pp.3282-3314.

[12] Zate, M., Raut, S., Shirsat, S.D., Sangale, A. and Kadam, A., **2020.** Ferrite nanostructures: Synthesis methods. In: *Spinel Ferrite Nanostructures for Energy Storage Devices. Elsevier*, pp.13-34.

[13] Pham, T.N., Huy, T.Q. and Le, A.-T., **2020.** Spinel ferrite (AFe_2O_4)-based heterostructured designs for lithium-ion battery, environmental monitoring, and biomedical applications. *RSC Advances*, 10, pp.31622-31661.

[14] Shobana, M., **2021.** Nanoferrites in biosensors—a review. *Materials Science and Engineering: B*, 272, p.115344.

[15] Sarac, M., **2020.** Magnetic, structural, and optical properties of gadolinium-substituted $Co_{0.5}Ni_{0.5}Fe_2O_4$ spinel ferrite nanostructures. *Journal of Superconductivity and Novel Magnetism*, 33, pp.397-406.

[16] Malaie, K., Heydari, Z. and Ganjali, M.R., **2021.** Spinel nano-ferrites as low-cost (photo) electrocatalysts with unique electronic properties in solar energy conversion systems. *International Journal of Hydrogen Energy*, 46, pp.3510-3529.

[17] Vinosha, P.A., Manikandan, A., Ragu, R., Dinesh, A., Thanrasu, K., Slimani, Y., Baykal, A. and Xavier, B., **2021.** Impact of nickel substitution on structure, magneto-optical, electrical and acoustical properties of cobalt ferrite nanoparticles. *Journal of Alloys and Compounds*, 857, p.157517.

[18] Rather, S.U., Bamufleh, H.S. and Alhumade, H., **2021.** Structural, thermal, morphological, surface, chemical, and magnetic analysis of Al^{3+}-doped nanostructured mixed-spinel cobalt ferrites. *Ceramics International*, 47, pp.17361-17372.

[19] Hussein, M.M., Saafan, S.A., Abosheiasha, H., Zhou, D., Klygach, D., Vakhitov, M., Trukhanov, S., Trukhanov, A., Zubar, T., Astapovich, K., **2023.** Crystal structure and peculiarities of microwave parameters of $Co_{1-x}Ni_xFe_2O_4$ nano spinel ferrites. *RSC Advances*, 13, pp.26879-26891.

[20] Sen, S.K., Barman, U.C., Manir, M., Mondal, P., Dutta, S., Paul, M., Chowdhury, M., Hakim, M., **2020.** X-ray peak profile analysis of pure and Dy-doped α-MoO3 nanobelts using Debye-Scherrer, Williamson-Hall and Halder-Wagner methods. *Advances in Natural Sciences: Nanoscience and Nanotechnology*, 11, p.025004.

[21] Talam, S., Karumuri, S.R. and Gunnam, N., **2012**. Synthesis, characterization, and spectroscopic properties of ZnO nanoparticles. *International Scholarly Research Notices*, *2012*(1), p.372505.

[22] Petrila, I. and Tudorache, F., **2021.** Effects of sintering temperature on the microstructure, electrical and magnetic characteristics of copper-zinc spinel ferrite with possibility use as humidity sensors. *Sensors and Actuators A: Physical*, 332, p.113060.

[23] Serry, F.M. and Schmit, J., **2019.** Characterization and Measurement of Microcomponents with the Atomic Force Microscope (AFM). *In: Optical Inspection of Microsystems. CRC Press*, pp.155-176.

[24] Iqbal, Z., Tanweer, M.S. and Alam, M., **2023.** Reduced graphene oxide-modified spinel cobalt ferrite nanocomposite: synthesis, characterization, and its superior adsorption performance for dyes and heavy metals. *ACS Omega*, 8, pp.6376-6390.

[25] Jeevanantham, B., Song, Y., Choe, H. and Shobana, M., **2021.** Structural and optical characteristics of cobalt ferrite nanoparticles. *Materials Letters*: X, 12, p.100105.

[26] Kamran, M. and Anis-ur-Rehman, M., **2022.** Resistive switching effect in RE-Doped cobalt ferrite nanoparticles. *Ceramics International*, 48, pp.16912-16922.

[27] Pydiraju, T., Rao, K.S., Rao, P.A., Varma, M.C., Kumar, A.S. and Rao, K., **2021.** Co-Cd nanoferrite for high frequency application with phenomenal rise in DC resistivity. *Journal of Magnetism and Magnetic Materials*, 524, p.167662.

[28] Badiger, H., Matteppanavar, S. and Hegde, B., **2023.** Structural, electrical and magnetic properties of low dimensional Pr-doped Co-Zn ferrite nanoparticles. *Journal of Superconductivity and Novel Magnetism*, 36, pp.675-684.

[29] Andhare, D.D., Patade, S.R., Kounsalye, J.S. and Jadhav, K., **2020.** Effect of Zn doping on structural, magnetic and optical properties of cobalt ferrite nanoparticles synthesized via. Co-precipitation method. *Physica B: Condensed Matter*, 583, p.412051.

[30] Divya, S., Sivaprakash, P., Raja, S.E., Muthu, I., Kim, N., Renuka, S. and Arumugam, T.H., **2022.** Impact of Zn doping on the dielectric and magnetic properties of $CoFe_2O_4$ nanoparticles. *Ceramics International*, 48, pp.33208-33218.

